IJST, Transactions of Mechanical Engineering, Vol. 38, No. M2, pp 389-402
Printed in The Islamic Republic of Iran, 2014

FULL COMPLIANT CONTINUUM ROBOTIC FINGER AND ITS KINEMATIC MODEL*

G. J. BAO[1], X. L. MA[2], X. Y. LUO[3], T. F. SHAO[4], L. B. ZHANG[5] AND Q. H. YANG[6**]

[1-3,5-6]Key Laboratory of E&M, Zhejiang University of Technology, Ministry of Education & Zhejiang Province, Hangzhou, 310032, China
Email: robot@zjut.edu.cn
[4]China Jiliang University, Hangzhou 310018, China

Abstract– Different from the traditional rigid robots made by hard material such as metal, continuum robots are bionic mechanisms which feature high compliance and continuous shape-changing ability. A full compliant continuum robotic finger is proposed, which is driven by the compressed air inside its silicon rubber chamber and has a certain degree of grasping rigidity. By the moment equilibrium analysis, the mathematical model for the inside compressed air pressure and the bending angle of the finger is established. The kinematic Cartesian coordinates for the proposed continuum robotic finger are constructed based on the D-H method. Then the kinematic model is derived. Simulation and experimental results showed that the proposed full compliant continuum robotic finger has abilities of continuous compliant shape-changing and movement, and the established kinematic model can describe the finger's movement process and its characteristics.

Keywords– Continuum robot, soft robot, robotic dexterous hand, pneumatic muscle actuator

1. INTRODUCTION

As the final executing mechanism interacting with the object, end-effector is a very essential factor for robotic system [1, 2]. Robotic multi-fingered dexterous hand, which features high adaptability, flexibility and multi-DOF (Degree of Freedom), can realize complex anthropopathic operations, such as grasping, holding and clipping [3-5]. Dexterous hand has broad prospects for application in aviation, deep sea exploration, medical rehabilitation, remote operation, serving the disabled and so on. So researchers pay close attention to this field. Most of the developed dexterous hands were made in rigid mechanical structure, such as the Utah/MIT hand [6] designed by the University of Utah and Massachusetts Institute of Technology, Robonaut hand [7, 8] developed by NASA, HIT/DLR hand [9] developed by Harbin Institute of Technology and the German Space Agency, and so on. These dexterous hands used metal or polymeric material with high rigidity and hardness to create the palm and fingers, and adopted motor, cable and pulley as the driving elements. Each single rigid finger can be taken as a classical serial robot. So the kinematics and inverse kinematics can be derived based on the classical D-H method. But the compliance and safety of the rigid dexterous hand are insufficient, especially for the soft and tender objects. Also, there is prominent problem of psychological safety in terms of interacting with biological objects.

With the development of bionics, a new type of robot, defined as continuum robot [10, 11], is proposed, which simulates the biological structures (such as elephant trunk and octopus arm) and

*Received by the editors October 8, 2013; Accepted February 3, 2014.
**Corresponding author

characteristics. Being opposite to the traditional rigid robots, continuum robots feature low rigidity, high compliance, curvature and adaptability. They can change their own shape according to the form of objects or the features of obstacles in unknown environments. Continuum robots are good at grasping and operating non-structural and tender objects. They have broad prospects of application in service robot, rehabilitation robot, agricultural robot, education robot, entertainment robot and rescue robot.

Continuum robots are mainly actuated by SMA (Shape Memory Alloys) or fluid. Compressed air driven continuum robots can fully express the continuity and compliance of their movement. Toshiba Corp. developed a four-fingered flexible hand [12] based on 3-DOF flexible microactuator, which can execute grasping, holding and twisting operation. The human hand-like ultra-light hand [13] based on flexible fluid driver can operate heteromorphosis objects due to its compliance in every joint. Walker and Jones developed a 3-DOF continuum robot Air-Octor [14], which is driven by three equispaced ropes and compressed air inside its chamber. They also designed an octopus tentacle like continuum robot: OctArm [15], driven by the typical McKibben pMA (pneumatic muscle actuator). Another 6-module continuum robot inspired by octopus arm was designed to simulate the creature's motion, with four pMAs driving each module [16]. Chen and Redarce proposed a pneumatic-driven flexible robotic manipulator ColoBot [17], driven by compressed air inside the three active pneumatic chambers regularly disposed at 120° apart in the rubber shell. Bi-bellows is an elastic tube with one half thicker than the other, which has compliant single DOF actuated by pneumatic system [18]. To resist the swelling of the elastic tube, rigid hoops were fixed along its 3D printed prototype. The untraceable friction between the hoops and bellows can be avoided by burying the reinforcing element into the actuator body [19], which was referenced in the design of FPA (flexible pneumatic actuator) [20], adopting a silicon rubber tube as its body with embedded spring.

All the above continuum robots have significant characteristics of continuous flexibility and curvature, but no rigidity for grasping or gripping, which limits their application in practice, such as fruit harvesting, tableware holding, feeding and so on. Based on the previous work [20], we proposed a full compliant continuum finger with a certain degree of rigidity, and its kinematic model is established. The paper is organized as follows. Section 2 introduces the structure and working principle of the full compliant continuum finger. The mathematical model for the inside compressed air pressure and the angle of curvature is established in section 3. The kinematic model is derived in section 4. The mathematical model is simulated in section 5 and verified by experiments in section 6. Section 7 shows the finger's application in cucumber harvesting robot. Finally, a conclusion is drawn in section 8.

2. STRUCTURE AND WORKING PRINCIPLE

a) Structure design

The structure of the proposed full compliant continuum robotic finger is shown in Fig. 1. The body of the finger is a silicon rubber tube, which has a thickened side and is sealed with two covers. A spring is embedded inside the rubber shell as the reinforcing rib. The thickened side has a built-in thin elastic steel strap, which can enhance the stiffness perpendicular to the bending plane. There is a venthole in one of the covers, which is the channel for air to inflate or deflate the finger chamber.

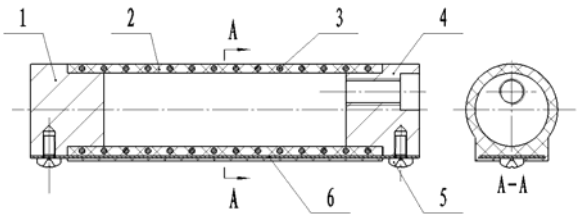

1,4 cover; 2 rubber tube; 3 spring; 5 bolt; 6 elastic steel strap
Fig. 1. Structure of the robotic finger

b) Working principle

The working principle of the proposed full compliant continuum robotic finger is as follows. Compressed air inflates the finger chamber through the venthole. The rubber tube shows little or no radial swelling because of the restraint of the spring. Then, driven by the compressed air, the thin side of the rubber tube will extend while the other thickened side will not because of the elastic steel strap. Thus the finger will bend to the thickened side, shown in Fig. 2. The bending angle increases with the air pressure inside the chamber. The finger will return to its original state driven by the elasticity of rubber and elastic steel strap when the chamber is deflated.

Because of the function of thickened shell and elastic steel strap, the finger will show a certain degree of stiffness and has no or less deformation when there is external load perpendicular to the bending plane. When grasping or operating an object, the thickened shell enhances the contacting area with object, which ensures the grasping stability. Furthermore, if necessary, angle and force transducer can be attached to the thickened side to sample and feed back motion information to the controller.

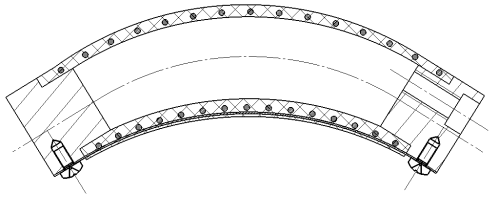

Fig. 2. Bending state of the finger

3. PRESSURE-ANGLE MODEL OF THE FINGER

As described above, the finger bends to the thickened side due to the compressed air inside the chamber. Its force analysis is shown in Fig. 3, where the finger can be taken as a Euler-Bernoulli Beam. According to Fig. 3a, the force equilibrium is:

$$F_h = F_p - F_b - F \tag{1}$$

where, F_h represents the tensile force at the rubber thickened side, N; F_b denotes the tensile force at the thin side, N; F_p is the force on the cover produced by the pressure difference between the inside compressed air and the atmosphere, N and F is the external load, N. Obviously,

$$F_p = \pi r_0^2 (p - p_{atm}) \tag{2}$$

where, p denotes the compressed air pressure inside the chamber, MPa; p_{atm} is the atmosphere pressure in MPa, and r_0 represents the average radius of the finger chamber, in mm.

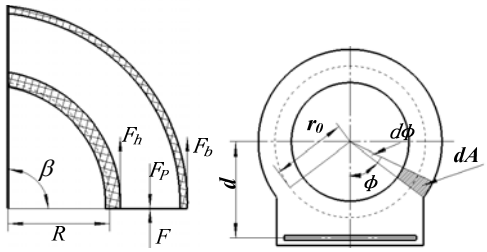

(a) force analysis (b) finger section
Fig. 3. Force analysis of the finger

The moment equilibrium at the center of the bended finger is:

$$M_h = M_p - M_b - M \tag{3}$$

where, M_h denotes the moment produced by F_h, N·m; M_b represents the moment produced by F_b, N·m; M_p is the moment produced by F_p and M is the moment produced by F, N·m.

$$M_p = F_p d \tag{4}$$

where d represents the distance from the finger chamber center to the elastic steel strap, mm.

During the bending motion of the finger, the radial deformation can be ignored according to the analysis in Ref. [21]. So the average radius of the finger chamber can be taken as a constant. According to Fig. 3b and the isovolumetric principle of material, the shell thickness t_ϕ at angle ϕ can be expressed by:

$$t_\phi = \frac{L_0}{L_\phi} t_0 \tag{5}$$

where, L_0 is the initial length of the finger, mm; L_ϕ is the length at angle ϕ, mm; t_0 is the initial shell thickness of the finger, mm.

The bended finger forms an arc, as shown in Fig. 3a. Then there is geometrical relationship:

$$L_0 = \beta R \tag{6}$$

$$L_\phi = \beta(d - r_0 \cos\phi + R) \quad (0 \le \phi \le \pi) \tag{7}$$

where, β is the bending angle of finger, rad; R is the radius of curvature at the elastic steel strap, mm.

The average strain at angle ϕ is:

$$\varepsilon = \frac{L_\phi - L_0}{L_0} \tag{8}$$

Due to the geometrical restraint, the stretch rate of the finger rubber tube is less than 100%, which means that the stress σ has linear relationship with the strain ε according to Hooke's law [22]. That is:

$$\sigma = E\varepsilon \tag{9}$$

where, E is the Young's modulus of the finger rubber tube, MPa.

In the cross section, the integral area dA at angle ϕ is:

$$\mathrm{d}A = t_\phi r_0 \mathrm{d}\phi \tag{10}$$

Then, the elastic force of the rubber on the area dA at angle ϕ can be written as:

$$\mathrm{d}F_b = \sigma \mathrm{d}A \tag{11}$$

Substituting (8), (9) and (10) into (11), we get the following expression:

$$\mathrm{d}F_b = E \frac{L_\phi - L_0}{L_0} t_\phi r_0 \mathrm{d}\phi \tag{12}$$

Substituting (5), (6) and (7) into (12), dF_b can be expressed as:

$$\mathrm{d}F_b = E \frac{d - r_0 \cos\phi}{d - r_0 \cos\phi + R} t_0 r_0 \mathrm{d}\phi \quad (0 \le \phi \le \pi) \tag{13}$$

Thus, the moment M_b in (3) can be written as:

$$M_b = 2\left[\int_0^\pi (d - r_0 \cos\phi + R)\mathrm{d}F_b\right] \tag{14}$$

When (13) is substituted into (14), M_b can be derived as:

$$M_b = 2\pi E t_0 r_0 d \tag{15}$$

Substituting (2), (4) and (15) into (3), we get the formula of M_h:

$$M_h = \pi r_0^2 (p - p_{\text{atm}}) d - 2\pi E t_0 r_0 d - M \tag{16}$$

According to Euler Bernoulli's theorem, M_h should also satisfy the following equation:

$$\frac{1}{R} = \frac{M_h}{E_1 I} \tag{17}$$

where, E_1 is the Young's modulus of the built-in elastic steel strap, MPa; I denotes the inertial moment of the strap at the neutral axis, mm^4.

Substituting (6) and (16) into (17), we can get:

$$\beta = \frac{\pi r_0^2 (p - p_{\text{atm}}) d - 2\pi E t_0 r_0 d - M}{E_1 I} L_0 \tag{18}$$

4. KINEMATIC MODEL

a) Motion analysis

Usually, the typical articulated robotic finger of rigid dexterous hands uses joint structure to connect links, shown in Fig. 4. The rigid links form the whole structure of the articulated finger and keep the relative distance between two adjacent joints. There is relative rotary motion only at the joints. The position and posture of the articulated finger are controlled through all the joints. When operating an object, all the joints need to work synergistically. Still the degree of freedom is directly determined by the limited number of the joints, and the compliance for non-structural objects is quite low, as clearly explained in Fig. 4b.

(a) initial state (b) grasping state

Fig. 4. Motion forms of articulated robot finger

Different from the traditional articulated dexterous fingers, the full compliant continuum finger has no discrete joints and rigid links. Actually, it works like the tail of shrimp, shown in Fig. 5. The continuum finger can reform itself according to the shape of objects, performing the excellent curvature ability which the articulated robot does not have. In nature, the proposed finger is a kind of interior-driven continuum robot [23]. When grasping an object, the continuum finger can realize continuous bending process, with the only power source of compressed air inflating its chamber, Fig. 5b.

(a) initial state (b) grasping state

Fig. 5. Motion forms of continuum finger

b) Posture model of the continuum finger tip

To simplify the model, the continuum finger is abstracted as a smooth continuous curve, as shown in Fig. 6.

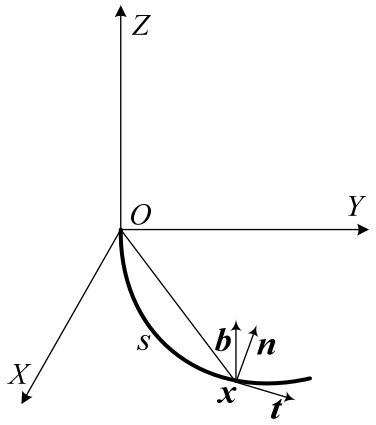

Fig. 6. Abstracted model of continuum finger

In Fig. 6, the continuum finger works in the *XOY* plane, the arbitrary point x can be represented by:

$$\boldsymbol{x} = \left[x, y, 0\right]^T \tag{19}$$

The unit tangent vector, unit normal vector and unit binormal vector of the arbitrary point *x* are represented by ***t***, ***n*** and ***b***, respectively. The three vectors are functions of the arc length *s*. According to the definition and Frenet-Serret formulas for spatial curve [24], we get:

$$\begin{cases} \boldsymbol{t} = \dfrac{d\boldsymbol{x}}{ds} \\ \boldsymbol{t} \cdot \boldsymbol{n} = 0 \\ \boldsymbol{b} = \boldsymbol{t} \times \boldsymbol{n} \\ \dfrac{d\boldsymbol{t}}{ds} = k\boldsymbol{n} \\ \dfrac{d\boldsymbol{n}}{ds} = -k\boldsymbol{t} + \tau\boldsymbol{b} \\ \dfrac{d\boldsymbol{b}}{ds} = -\tau\boldsymbol{n} \end{cases} \tag{20}$$

where, *s* represents the length of arc *ox*; *k* is the curvature of arc *ox* and τ stands for the torsion of arc *ox*.

c) Differential transformation of the posture coordinates

As mentioned in section 2, there is no or less deformation in the plane perpendicular to the bending plane. Therefore $\boldsymbol{\tau}$=0, and (20) can be simplified as:

$$\boldsymbol{t}'' + k^2\boldsymbol{t} = 0 \tag{21}$$

Formula (21) satisfies the following initial conditions:

$$\boldsymbol{t}_0 = \boldsymbol{t}(0) \ ; \ \boldsymbol{n}_0 = \boldsymbol{n}(0) \tag{22}$$

Substituting (22) into (21), we get:

$$\boldsymbol{t}(s) = \boldsymbol{t}_0 \cos(ks) + \boldsymbol{n}_0 \sin(ks) \tag{23}$$

Integrating (23) results in:

$$\boldsymbol{x}(s) = \frac{\boldsymbol{t}_0}{k}\sin(ks) + \frac{\boldsymbol{n}_0}{k}\left[1-\cos(ks)\right] \tag{24}$$

According to (20) ~ (22), t_0 and n_0 can be written as:

$$\boldsymbol{t}_0 = \left[t_{0x}\ , t_{0y}\right]^T\ ;\ \boldsymbol{n}_0 = \left[-t_{0y}\ , t_{0x}\right]^T \tag{25}$$

Substituting (25) into (24), we get:

$$\begin{aligned}\left[x, y\right]^T = &\frac{1}{k}\left[t_{0x}\ , t_{0y}\right]^T \sin(ks) \\ &+\frac{1}{k}\left[-t_{0y}\ , t_{0x}\right]^T \left[1-\cos(ks)\right]\end{aligned} \tag{26}$$

The module of posture vector x is:

$$\left\|\boldsymbol{x}\right\| = \sqrt{x^2 + y^2} \tag{27}$$

where,

$$\begin{cases} x^2 = \dfrac{1}{k^2}t_{0x}^2 \sin^2(ks) - \dfrac{1}{k^2}t_{0x}t_{0y}\sin(ks)\left[1-\cos(ks)\right] \\ \qquad + \dfrac{1}{k^2}t_{0y}^2\left[1-2\cos(ks)+\cos^2(ks)\right] \\ y^2 = \dfrac{1}{k^2}t_{0y}^2 \sin^2(ks) + \dfrac{1}{k^2}t_{0x}t_{0y}\sin(ks)\left[1-\cos(ks)\right] \\ \qquad + \dfrac{1}{k^2}t_{0x}^2\left[1-2\cos(ks)+\cos^2(ks)\right] \end{cases} \tag{28}$$

Substituting (28) into (27), x is expressed as:

$$\left\|\boldsymbol{x}\right\| = \frac{\sqrt{2}}{k}\sqrt{1-\cos(ks)} \tag{29}$$

The angle between the posture vector x and the unit tangent vector t is defined as θ. From Fig.7, the trigonometric sine and cosine expressions are:

$$\sin(\theta) = \frac{\left\|\boldsymbol{x}\times\boldsymbol{t}_0\right\|}{\left\|\boldsymbol{x}\right\|\cdot\left\|\boldsymbol{t}_0\right\|} = \sqrt{\frac{1-\cos(ks)}{2}} \tag{30}$$

$$\cos(\theta) = \frac{\boldsymbol{x}\cdot\boldsymbol{t}_0}{\left\|\boldsymbol{x}\right\|\cdot\left\|\boldsymbol{t}_0\right\|} = \frac{\sin(ks)}{\sqrt{2(1-\cos(ks))}} \tag{31}$$

Multiplying (30) with (31), we get:

$$\theta = \frac{ks}{2} \tag{32}$$

Substituting (32) into (29), we get:

$$\left\|\boldsymbol{x}\right\| = \frac{s}{\theta}\sin(\theta) \tag{33}$$

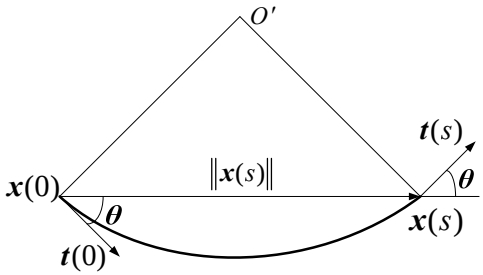

Fig. 7. Posture vector $\boldsymbol{x}$

d) Kinematic model for continuum finger

In 1955, Denavit and Hartenberg proposed the classical kinematics D-H method for the traditional articulated robots [25]. The continuum finger cannot directly use the D-H method for kinematic analysis because of its special structure and working principle. Here, we establish a new coordinate based on the D-H Cartesian coordinate system [26] for the proposed continuum finger, shown in Fig.8. $O_0X_0Y_0Z_0$ is a fixed coordinate which is attached to the base point O of the continuum finger, while all the others are moving coordinates. The static coordinate $O_0X_0Y_0Z_0$ and moving coordinate $O_1X_1Y_1Z_1$ share the same base point $O_0(O_1)$. Also, the moving coordinates $O_1X_1Y_1Z_1$ and $O_2X_2Y_2Z_2$ share the same base point $O_2(O_3)$. In Fig.8, all the Z axes Z_1, Z_2 and Z_3 are perpendicular to the paper and point to the outside.

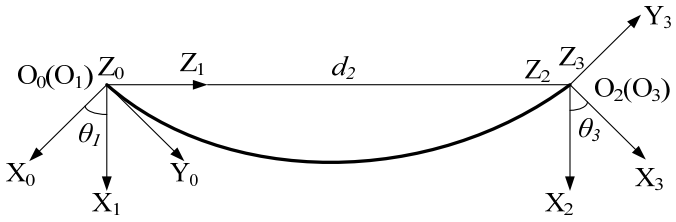

Fig. 8. Coordinates for the continuum finger

From Fig. 8, the revised D-H coordinates have four parameters:
θ_j: Angle from X_i to X_j rotating around Z_i, positive when counter-clockwise; d_j: Distance from axis X_i to X_j, positive when consistent with the positive direction of axis Z_i; a_j: Distance from Z_i to Z_j, positive when consistent with the positive direction of axis X_j; α_{ij}: Angle from Z_i to Z_j rotating around X_j, positive when counter-clockwise.

Then the revised D-H parameters for the continuum finger are listed in Table 1.

Table 1. Revised D-H parameters

	θ_j /(°)	d_j /mm	a_j /mm	α_{ij} /(°)
0-1	θ_1	0	0	-90
1-2	0	d_2	0	90
2-3	θ_3	0	0	0

From Figs. 7 and 8, we can get:

$$\begin{cases} \theta_1 = \theta_3 = \theta \\ d_2 = \|\boldsymbol{x}\| \end{cases} \tag{34}$$

According to the parameters in Table 1 and formula (34), the homogeneous transformation between the different coordinates can be written as follows:

$$A_0^1 = Rot(z,\theta_1)Rot(x,\alpha_{01}) = \begin{bmatrix} \cos\theta & 0 & -\sin\theta & 0 \\ \sin\theta & 0 & \cos\theta & 0 \\ 0 & -1 & 0 & 0 \\ 0 & 0 & 0 & 1 \end{bmatrix} \tag{35}$$

$$A_1^2 = Trans(0,0,d_2)Rot(x,\alpha_{12}) = \begin{bmatrix} 1 & 0 & 0 & 0 \\ 0 & 0 & -1 & 0 \\ 0 & 1 & 0 & \|\boldsymbol{x}\| \\ 0 & 0 & 0 & 1 \end{bmatrix} \tag{36}$$

$$A_2^3 = Rot(z,\theta_3)Rot(x,\alpha_{23}) = \begin{bmatrix} \cos\theta & -\sin\theta & 0 & 0 \\ \sin\theta & \cos\theta & 0 & 0 \\ 0 & 0 & 1 & 0 \\ 0 & 0 & 0 & 1 \end{bmatrix} \tag{37}$$

From (35), (36) and (37), the posture equation for arbitrary point $\boldsymbol{x}$ of the continuum finger in the fixed coordinate $O_0X_0Y_0Z_0$ can be written as:

$$A_0^3 = A_0^1 A_1^2 A_2^3 = \begin{bmatrix} \boldsymbol{R} & \boldsymbol{x} \\ 0 & 1 \end{bmatrix} \tag{38}$$

where,

$$\boldsymbol{R} = \begin{bmatrix} \cos(ks) & -\sin(ks) & 0 \\ \sin(ks) & \cos(ks) & 0 \\ 0 & 0 & 1 \end{bmatrix} \tag{39}$$

$$\boldsymbol{x} = [x, y, 0]^T = \left[\frac{1}{k}(\cos(ks)-1) \quad \frac{1}{k}\sin(ks) \quad 0\right]^T \tag{40}$$

5. MODEL SIMULATION

According to the established kinematic model, the axial extension and curvature angle are calculated using Matlab. Then the tracks of the continuum finger are drawn in Fig. 9. The parameters used in the simulation are listed in Table 2.

Table 2. Simulation parameters

Parameter	Value
Average radius of rubber tube r_0/mm	5
Initial shell thickness of tube t_0/mm	2
Initial length of tube L_0/mm	100
Young's modulus of tube E/MPa	2.5
Atmosphere pressure p_{atm}/MPa	0.1
Young's modulus of steel strap E_1/GPa	200

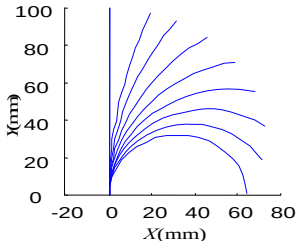

Fig. 9. Calculated tracks of finger motion

6. EXPERIMENT AND ANALYSIS

a) Experimental setup

Experiments were designed to vary the pressure-angle relationship and the established kinematic model. The system configuration is shown in Fig. 10. The continuum finger is driven by compressed air coming from the air tank running through the filter valve, oil mist separator and proportional regulator. The air pressure that inflated the finger chamber is controlled by the computer via the data acquisition board, digital analog converter (D/A) and proportional regulator. The real-time actual air pressure inside the finger chamber is sampled by the analog digital converter (A/D). A micro industrial digital camera MV-3000UC was adopted in the experiments to record the motion of the continuum finger. Then the bending angle and position of the finger were calculated in CAD software, shown in Fig. 11.

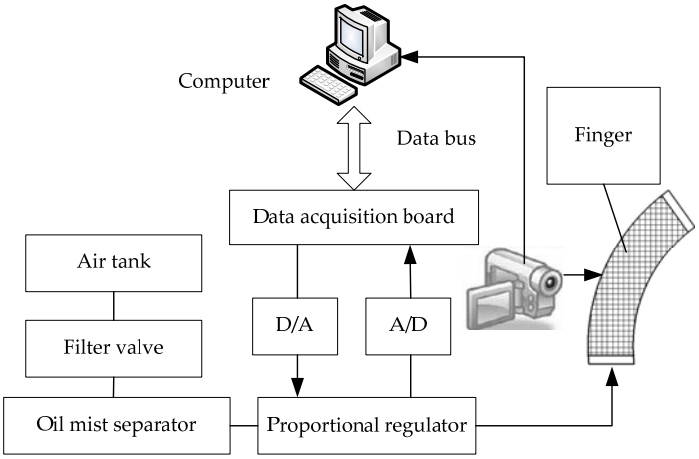

Fig. 10. Experimental setup for continuum finger

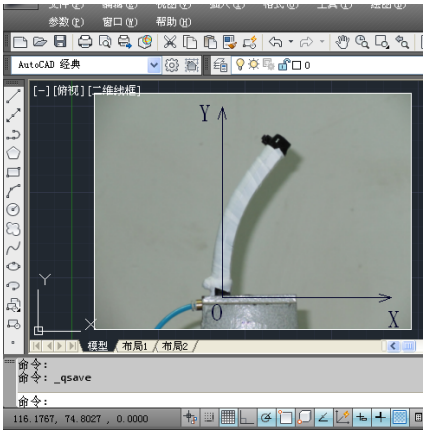

Fig. 11. Angle and position measuring in CAD software

b) Result and discussion

The static experiment was done to reveal the relationship between the air pressure p inside the chamber and the bending angle β of the full compliant continuum robotic finger. The experimental data are compared with the theoretical curve produced by equation (18), shown in Fig. 12. As can be noted, that there is a hysterisis loop between the inflation and deflation process. This is caused by the viscosity of the silicon rubber. Another problem is that all the experimental bending angles are smaller than their counterparts calculated by equation (18). As described in Section 3, in the pressure-angle model, we did not take into account the radial deformation of the silicon rubber and effect of the elastic steel strap. Although ignoring these factors makes the pressure-angle model reasonable and simply, it results in the fact that the actual pressure-angle curves are lower than the simulated one. Despite the deviations, the mathematical model can describe the pressure-angle property of the proposed full compliant continuum robotic finger.

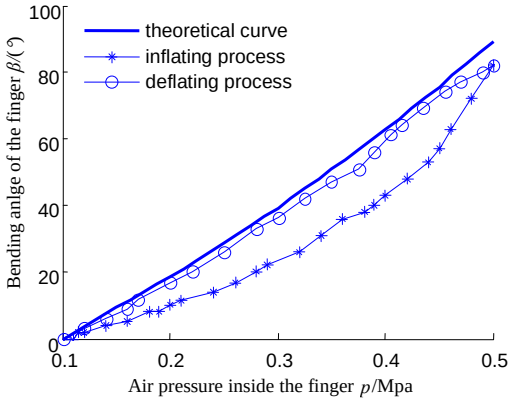

Fig. 12. Pressure-angle relationship of experiment and simulation

The experimental data of the fingertip position is compared with the simulation result, shown in Fig. 13. To make it easy for the evaluation of the established kinematic model, the data of inflating and deflating process are merged. That is, each experimental data point stands for the average value of inflating and deflating process. From the contrastive curve of experiment and simulation, it can be concluded that the established theoretical model can properly describe the continuum finger's static behavior, with the max error of 6.2mm in X-direction and 8.1mm in Y-direction.

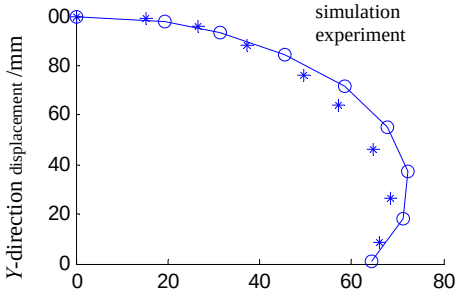

Fig. 13. Experiment and simulation data of the finger tip's position

c) Analysis of accuracy and compliance

Although the feasibility of the mathematical model was verified by experiment, there exist quite large errors between the simulation and experimental data, which is not acceptable in traditional rigid robot. The low accuracy of the proposed continuum finger inheres from its soft structure and rubber material. Also,

there are factors influencing the pressure-angle model and kinematic model, such as nonuniformity of the material and structure, deviation of Young's modulus of the rubber tube and steel strap, which are immeasurable and ignored in the model derivation process. Another reason for the error is the assumption that the continuum finger will bend and form an arc of a circle when inflated with compressed air. In fact, it may not curve to a circular fashion because of non-equally distributed pneumatic pressure inside the chamber, concentrated load or multi-pointed load from non-circular object.

However, accuracy is not the most important technique indicator for continuum robot, while compliance is the initial incentive and final goal. Compliance can overcome the approaching and operating difficulties caused by the precision of the traditional robot in non-structured environment and objects. Furthermore, flexibility and low accuracy enable the continuum finger to interact with objects whose nature, mechanical property and behavior are not clear, such as agricultural products, animal and human beings. As it were, continuum robots are not designed to replace the rigid robots, but to do what they cannot do and explore new application fields of robots.

7. IMPLEMENTATION

An end-effector for cucumber harvesting robot was developed employing three continuum fingers. The air pressure inside the chambers of the three continuum fingers is controlled by the same pneumatic proportional regulator, which can theoretically ensure that they perform the same working process and behavior. Indoor experimental photo shown in Fig. 14 implies that the developed three-fingered grasping end-effector can handle a cucumber without any force or stress transducer. Firstly, the vision module identified and located the cucumber from the plant. Then the robot approached and grasped the cucumber with the three-fingered end-effector. The three continuum fingers can hold the cucumber tightly but gently, without hurting the fruit. Additionally, a link chain was attached to each continuum finger to enforce the stiffness of the whole structure, avoiding its undesired deformation in the gravity direction in the case that the embedded elastic steel strap cannot provide sufficient rigidity.

(a) cucumber harvesting robot (b) enlarged end-effector

Fig. 14. Three-fingered cucumber harvesting end-effector

8. CONCLUSION

Taken from our previous work, a new type of full compliant continuum robotic finger is proposed. The continuum finger extends and curves like shrimp tail, driven by the pneumatic pressure inside its chamber. The mathematical model for the curvature angle and the driven air pressure is derived based on moment equilibrium. Unlike the traditional rigid articulated robot, the continuum finger has continuous deformation and motion along its body. So we adopt differential transform matrix to describe the posture of its tip. Revised coordinates are established on the rigid D-H coordinate system to develop the kinematic

model. The pressure-angle relationship and tip position tracking experiments verified the theoretical work and mathematical models. An implementation in cucumber harvesting end-effector is introduced to show the practicability of the proposed continuum finger.

Acknowledgement: This work is financially supported by the National Natural Science Foundation of China (granted No.51405441) and Natural Science Foundation of Ningbo China (granted No. 2013A610154).

REFERENCES

1. Bicchi, A. & Kumar, V. (2000). Robotic grasping and contact: a review. *2000 IEEE International Conference on Robotics and Automation*, April 24-28, San Francisco, CA, USA, Vol. 1, pp, 348-353.
2. Peter, O., Ye, Z. M., Jiang, H. Z., Yang, C. F. & Han, J. W. (2011). Formulation and evaluation of coupling effects between DOF motions of hydraulically driven 6 DOF parallel manipulator. *Iranian Journal of Science & Technology, Transaction B: Engineering*. Vol. 35, No. 2, pp. 143-175.
3. Jiang, L., Cai, H. G. & Liu, H. (2004). New type integrated humanoid finger and its dynamics analysis. *Chinese Journal of Mechanical Engineering*, Vol. 40, No. 4, pp. 139-143.
4. Zhang, L. B., Yang, Q. H., Xu, F., Bao, G. J. & Ruan, J. (2004). Review of research on multi-fingered robot hand and its driving system. *Transactions of the CSAE*, Vol. 20, No. 3, pp, 271-274.
5. Stankovski, S., Ostojic, G., Tarjan, L., Skrinjar, D. & Lazarevic, M. (2011). IML robot grasping process improvement. *Iranian Journal of Science & Technology, Transaction B: Engineering*. Vol.35, No.1, pp 197-207.
6. Jacobsen, S., Wood, J., Knutti, D. & Biggers, K. B. (1984). The Utah/MIT dexterous hand: work in progress. *The International Journal of Robotics Research*, Vol. 3, No. 4, pp, 21-50.
7. Engelberger, G. (2001). NASA's Robonaut. *Industrial Robot: An International Journal*, Vol. 28, No.1, pp, 35 - 42.
8. Diftler, M. A., Mehling, J. S., Abdallah, M. E. & Radford, N. A. (2011). Robonaut 2 - the first humanoid robot in space. *2011 IEEE International Conference on Robotics and Automation*, May 9-13, Shanghai China, pp, 2178 - 2183.
9. Liu, H., Meusel, P., Hirzinger, G. & Jin, M. H. (2008). The Modular Multisensory DLR-HIT-Hand: Hardware and Software Architecture. *Mechatronics, IEEE/ASME Transactions on*, Vol. 13, No. 40, pp, 461 – 469.
10. Calisti, M., Giorelli, M. & Laschi, C. (2012). A locomotion strategy for an octopus-inspired octopus. *Biomimetic and Biohybrid Systems*, Vol. 7375, pp, 337-338.
11. Calisti, M., Giorelli, M., Levy, G., Mazzolai, B., Hochner, B., Laschi, C. & Dario, P. (2011). An octopus-bioinspired solution to movement and manipulation for soft robots. *Bioinspiration & Biomimetics*, Vol. 6, No. 3, pp, 1-10.
12. Suzumori, K., Iikura, S. & Tanaka, H. (1992). Applying a flexible microactuator to robotic mechanisms. *IEEE Control Systems*, Vol. 12, No. 1, pp, 21-27.
13. Schulz, S., Pylatiuk, C. & Bretthauer, G. (2001). A new ultralight anthropomorphic hand. *2001 IEEE International Conference on Robotics & Automation*, May 21-26, Seoul, Korea, Vol.3, pp. 2437-2441.
14. Mcmahan, W., Jones, B. A. & Walker, I. D. (2005). Design and implementation of a multi-section continuum robot; Air-Octor. *2005 IEEE/RSJ International Conference on Intelligent Robots and Systems*, August 2-2, Piscataway, NJ, USA, pp, 2578-2585.
15. Neppalli, S., Jones, B. A. & Mcmahan, W. (2007). OctArm – A soft robotic manipulator. *2007 IEEE/RSJ International Conference on Intelligent Robots and Systems*, Oct. 29 - Nov. 2, San Diego, CA, USA, pp, 2569.
16. Kang, R., Branson, D., Zheng, T., Guglielmino, E. & Caldwell, D. (2013). Design, modeling and control of a

pneumatically actuated manipulator inspired by biological continuum structures. *Bioinspiration & Biomimetics*, Vol. 8, pp: 036008 (14 pp).

17. Chen, G., Pham, M. T. & Reduarce, T. (2009). Sensor-based guidance control of a continuum robot for a semi-autonomous colonoscopy. *Robotics and Autonomous Systems*, Vol. 579, No. 6/7, pp, 712-722.
18. Shapiroa, Y., Wolfa, A. & Gaborb, K. (2011). Bi-bellows: Pneumatic bending actuator. *Sensors and Actuators A: Physical*, Vol. 167, No. 2, pp, 484–494.
19. Suzumori, K., Endo, S., Kanda, T., Kato, N. & Suzuki, H. (2007). A bending pneumatic rubber actuator realizing soft-bodied manta swimming robot. *2007 IEEE International Conference on Robotics and Automation*, April 10 - 14, Roma, Italy, pp. 4975–4980.
20. Yang, Q. H., Zhang, L. B., Bao, G. J. & Ruan, J. (2004). Research on novel flexible pneumatic actuator FPA. *2004 IEEE Conference on Robotics, Automation and Mechatronics*, December 1-3, Singapore, pp, 385-389.
21. Bao, G. J., Shao, T. F. & Li, S. H. (2011). Static model of flexible pneumatic swaying joint. *Transactions of the Chinese Society for Agricultural Machinery*, Vol. 42, No. 6, pp, 198-202, 212.
22. Treloar, L. R. G. (2005). *The physics of rubber elasticity*. New York: Oxford University Press.
23. Godage, I. S., Branson, D. T., Guglielmino, E., Medrano-Cerda, G. A. & Caldwell, D. G. (2011). Shape function-based kinematics and dynamics for variable length continuum robotic arms. *2011 IEEE International Conference on Robotics and Automation*, May 9 - 13, Shanghai, China, pp, 452-457.
24. Reza, R. (2009). Robot arm motion design by Frenet-Serret and rotation minimizing frames. *2009 IEEE International Conference on Computer Science and Information Technology*, July 25 – 26, Beijing, China, pp, 151-155.
25. Denavit, J. & Hartenberg, R. S. (1955). A kinematic notation for lower-pair mechanisms based on matrices. *Trans ASME J. Appl. Mech.*, No. 6, pp, 215–221.
26. Bryan, A. J. & Ian, D. W. (2006). Kinematics for multisection continuum robots. *IEEE Transactions on Robotics*, Vol. 22, No. 1, pp, 43-55.